Journal of Hazardous Materials 164 (2009) 592–599

Contents lists available at ScienceDirect

Journal of Hazardous Materials

journal homepage: www.elsevier.com/locate/jhazmat

Gas chromatographic study of degradation phenomena concerning building and cultural heritage materials

E. Metaxa, T. Agelakopoulou, I. Bassiotis, Ch. Karagianni, F. Roubani-Kalantzopoulou*

School of Chemical Engineering, National Technical University of Athens, 9 Iroon Polytechniou St., 157 80 Zografou, Athens, Greece

ARTICLE INFO

Article history:
Received 22 April 2008
Received in revised form 5 June 2008
Accepted 13 August 2008
Available online 20 September 2008

Keywords:
Statue degradation study
Deterioration of monuments
Physicochemical study of deterioration
Degradation inside museums

ABSTRACT

Air pollution influences all aspects of social and economical life nowadays. In order to investigate the impact of air pollution on materials of works of art, the method of Reversed Flow–Inverse Gas Chromatography has been selected. The presence of various atmospheric pollutants is studied on marbles, oxides—building materials and samples of authentic statues from the Greek Archaeological Museums of Kavala and of Philippi. The method leads to the determination of several physicochemical quantities and the characterization of the heterogeneous surfaces of these solids. Moreover, the influence of a second pollutant (synergistic effect) is examined. The structure, the properties and the behavior of the materials are examined by X-Ray Diffraction, Scanning Electron Microscopy and Raman Spectroscopy. Therefore, the precise measurement of the above mentioned quantities form the scientific basis for elucidation of the mechanism of the whole phenomenon of the degradation, thus providing a scientific platform to conservation procedures.

1. Introduction

Air pollution has increased dramatically the last decades. Major sources of air pollution are the exhaust gases from vehicles, power plants and heaters from apartments. Global warming, deterioration of forests, pollution of water basins are some of the sequences. Moreover, an important question arises from the influence of gas pollutants on the surfaces of various monuments and works of art [1,2].

Air pollution is essentially caused by sulphur and nitrogen oxides as well as hydrocarbons which are emitted into the atmosphere by sources related to industry, transportation and heating. The quality of indoor air in museums as far as the presence of potentially aggressive species such as SO_2, NO_x and O_3 is usually characterized through concentration measurements easily made by means of automatic instrumentation. Typical results of measurements for the mentioned pollutants and comparisons of indoor–outdoor pollution in museums, libraries and archives have been reported in review articles by Baer and Banks [1] and, more recently, by Bimblecombe [2]. These species are sometimes transformed, through complex reaction pathways, into others more aggressive ones. As far as air pollutants are concerned an important process which contributes to the damage of artworks is pollutant deposition and adsorption. Adsorption is a pure physicochemical phenomenon [3,4].

Qualitative evidence from monuments and buildings in industrialized countries indicates that rates of stone deterioration rise in the presence of urban and industrial pollutants. Measurements, which took place in Australia on surface reduction of marble tombstones, show that mean weathering rates have increased over the period 1885–1955. Weathering rates were lower before the establishment of sulphur dioxide-emitting plants [5].

In parallel, the effects of nitrogen dioxide on three calcareous stones (Pentelic marble, Portland limestone and Baumberger sandstone), used extensively in historic buildings, have been investigated under different conditions of relative humidity, mass of stone and grain size of stone. It was found that all three stones are not good sinks for NO_2. Pentelic marble and Portland limestone exhibit relatively low vulnerability to NO_2 and this does not vary with relative humidity significantly [6].

Furthermore, the objective of an interesting study was to compare the concentration of some air pollutants relevant to deposition, in an important Italian Gallery (Galleria degli Uffizi) [7]. Other remarkable studies are those concerning the environmental influence on several known monuments [8–10].

The reactivity of CaO(s) is believed to be strongly surface-dependent. The porosities of calcined $CaCO_3$ and $Ca(OH)_2$, have been shown to increase by 35–40% and to react more rapidly than non-porous CaO. The property of calcined limestone to react with SO_2 at elevated temperatures to form calcium sulphate is well

* Corresponding author. Tel.: +30 210 772 3277; fax: +30 210 20 27 691.
E-mail address: roubanif@central.ntua.gr (F. Roubani-Kalantzopoulou).

0304-3894/$ – see front matter © 2008 Elsevier B.V. All rights reserved.
doi:10.1016/j.jhazmat.2008.08.114

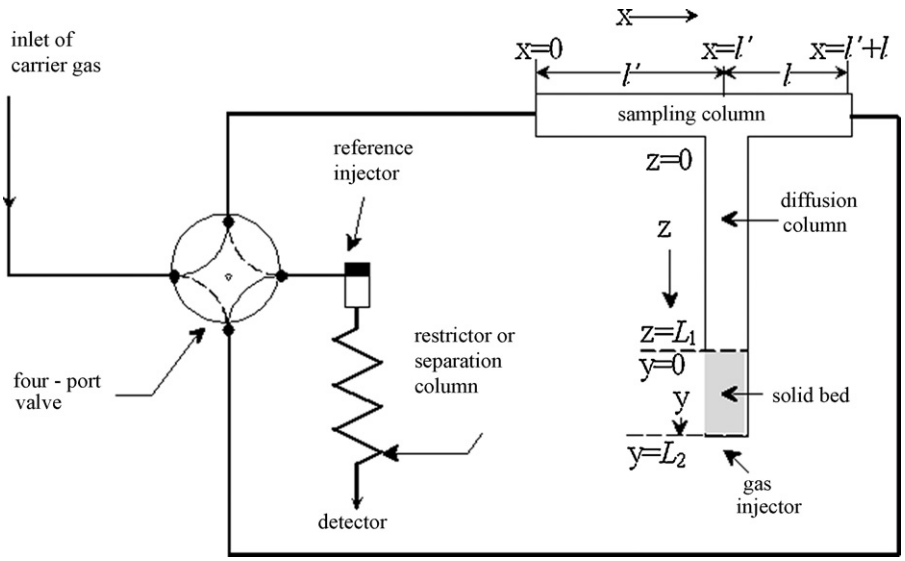

Fig. 1. Experimental setup of RF-IGC.

known and it is exploited in coal furnaces to reduce the SO_2 concentration in the flue gas [11].

A precise contribution to the elucidation of the mechanism of the deterioration of marbles and other building materials as well as metal oxide pigments of various works of art in museums has recently been published [12–14].

A suitable method, the so called Reversed Flow–(Inverse) Gas Chromatography (RF-IGC or RF-GC), has been selected in order to study in depth the air pollution impact, by studying adsorption and desorption phenomena of gases on solids [15–17]. Several important physicochemical quantities are determined, as local adsorption energy, local adsorption isotherm, local monolayer capacity, density probability function, local adsorption equilibrium concentration and energy from lateral interactions. The determination of all these physicochemical quantities is based on an appropriate mathematical model [18–21]. This simple method has been proved accurate and in contrast to classical Gas Chromatography, it is interested in solid properties and the physicochemical characterization of heterogeneous surfaces. Furthermore, time resolved analysis is achieved, providing detailed investigation of phenomena and mechanisms [22–24].

In this paper the impact of aliphatic hydrocarbon C_2-C_4 on building materials (marbles, oxides) and samples of authentic statues from the Greek Archaeological Museums of Kavala and of Philippi is investigated. Furthermore, the coexistence of a second pollutant (O_3, SO_2) is also studied.

2. Materials and methods

2.1. Experimental arrangement of RF-IGC

Gas chromatography instrumentation, somehow modified [3], can be used in order to determine the solid deterioration. The experimental arrangement is shown in Fig. 1. The whole sampling cell is accommodated inside the oven of a gas chromatograph Shimadzu GA-8A, having temperature control accuracy 1 °C. Thus, a small quantity of gas was injected into the column L_2. In the experiments for the synergistic effects of ozone and sulphur dioxide, this second pollutant was injected through the same column. Typical chromatograms obtained are shown in Figs. 2–4.

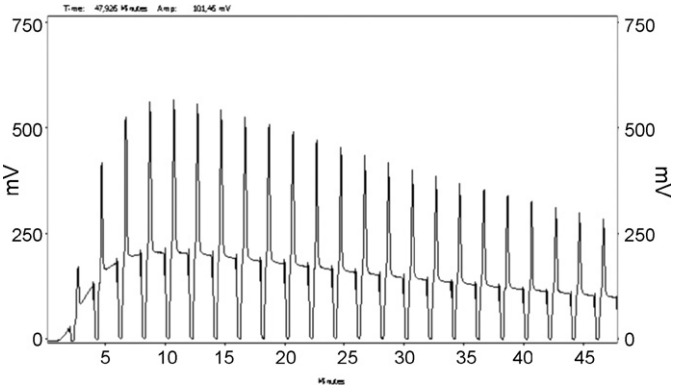

Fig. 2. Chromatogram of RF-IGC for the system C_2H_2/Statue L291 of Kavala, Greece.

2.2. Procedure of RF-IGC

Naturally the sampling procedure will give continuous asymmetric chromatographic signals, owing to the slow diffusion of the pollutants species out of the diffusion column. The RF-IGC method consists in reversing the direction of the carrier gas flow through the sampling column for a short time interval, by turning the valve from one position (Fig. 1, solid lines) to the other (Fig. 1, broken

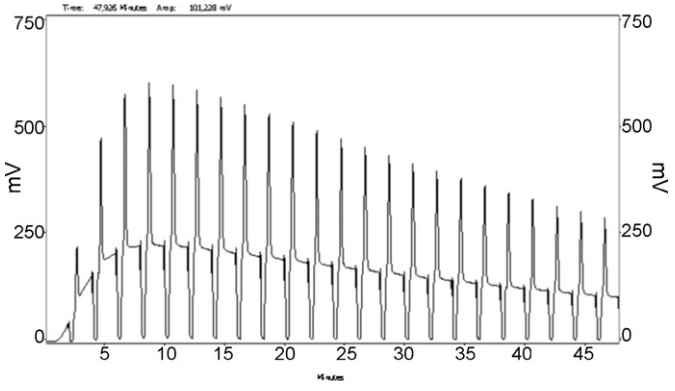

Fig. 3. Chromatogram of RF-IGC for the system C_2H_4/Statue L291 of Kavala, Greece.

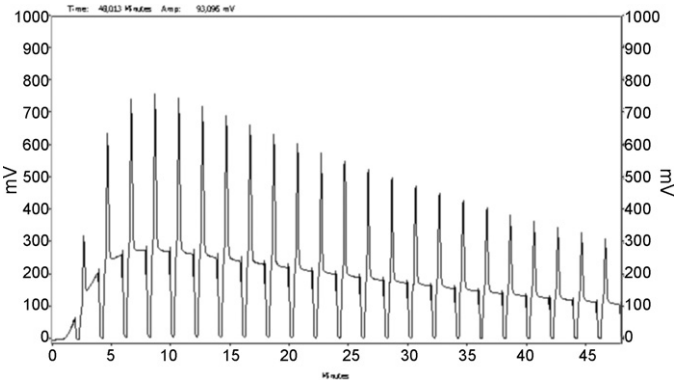

Fig. 4. Chromatogram of RF-IGC for the system C_2H_6/Statue L291 of Kavala, Greece.

lines), and vice versa. If the reversal time above is smaller than the dead time in the sampling column, each flow reversal creates one extra chromatographic peak (or more than one), which is a measure of the concentration at $x = l'$ (Fig. 1), at the time when the reversal was made.

2.3. Other methods

(1) X-Ray Diffraction (Siemens D5000 diffractometer with nickel-filtered CuKα_1 radiation (1.5405 Å), 40 kV and 30 mA)
(2) Scanning Electron Microscopy (Jeol 6100)
(3) Raman Spectroscopy (Nicolet Almega dispersive Raman system).

2.4. Materials

The systems examined are of the type A/X, B/X and A/B/X, where

- A: corresponds to one aliphatic hydrocarbon C_2-C_4, saturated or unsaturated (C_2H_6 99.95%, C_2H_4 99.5%, C_2H_2 99.6%, C_3H_6 99.4%, 1-C_4H_8 99.0%, all products of Air-Liquide, Hellas)
- B: is an inorganic gas O_3 (Ozoneur OZ1-L, Ozonia Int., Greece) or SO_2 (99.99%, Air-Liquide, Hellas)
- X: is the solid adsorbent, i.e. building materials (Pentelic marble, CaO, SiO_2 (M300), SiO_2 (M0010)) as well as sample of statues kindly supplied by the Greek Archeological museums of Kavala and Philippi (L291 and L351 of Kavala, L1991 of Philippi). Pentelic marble was a recently cut sample from Penteli's mountain ore. The oxides used were obtained from the Greek company Adamacopoulos S.A., 10–30 mesh, and had a purity of 99%.

The carrier gas in all cases was nitrogen 99.0% from Air-Liquide, Hellas.

3. Theory—calculation

The calculation of all physicochemical quantities has been performed using recently published models [3].

The main equation is Eq. (1)

$$H^{1/M} = gc(l',\ t) = \sum_{i=1}^{4} A_i\ \exp(B_i t)t \tag{1}$$

where H: height of sample peaks resulting from the flow reversal, cm. M: response factor of the detector, dimensionless. g: calibration factor of the detector, cm (mol cm^{-3})$^{-1}$; $c(l', t)$: measured sampling concentration of the pollutant (e.g. benzene) at $x = l'$ (mol cm^{-3}).

The explicit calculation of the adsorption parameters for the gases studied can be carried out in an analogous way to the one described earlier. All parameters refer to the values of c_y (0, t), i.e. the concentration of the gaseous pollutant at $y = 0$:

$$c_y(0,\ t) = \frac{\nu L_1}{D_z} c(l',\ t) = \frac{\nu L_1}{gD_z} \sum_{i=1}^{4} A_i\ \exp(B_i t) \tag{2}$$

where ν is the linear velocity of the carrier gas (cm s^{-1}) in the sampling column, L_1 the length of the diffusion column (cm) and D_z the diffusion coefficient of each hydrocarbon pollutant into the nitrogen carrier gas (cm^2 s^{-1}). From this, the value of the adsorbed concentration c_s^* is calculated

$$c_s^* = \frac{\alpha_y}{\alpha_s} k_1 \frac{\upsilon L_1}{gD_z} \sum_{i=1}^{4} \frac{A_i}{B_i} [\exp(B_i t) - 1] \tag{3}$$

where the first fraction corresponds to the ratio of the cross sectional area of the void diffusion column (cm^2) to the amount of solid adsorbent per unit length of the same column (g cm^{-1}), k_1 is the local adsorption coefficient, and the rest of the symbols have been explained after Eq. (2). The local adsorption isotherm is given by

$$\theta_t = \frac{c_s^*}{c_{\max}^*} \tag{4}$$

where $c_{\max}^*$ is the local monolayer capacity, and c_s^* is given by Eq. (3).

$$c_{\max}^* = c_s^* + \frac{\partial c_s^* / \partial c_y}{KRT} \tag{5}$$

Thus, for the $c_{\max}^*$ determination the above derivative and KRT from Eqs. (6) and (7), respectively, are needed

$$\frac{\partial c_s^*}{\partial c_y} = \frac{a_y}{a_s} k_1 \frac{\sum_{i=1}^{4} A_i\ \exp(B_i t)}{\sum_{i=1}^{4} A_i B_i\ \exp(B_i t)} \tag{6}$$

$$KRT = \frac{gD_z}{\upsilon L_1} \left\{ \frac{\sum_{i=1}^{4} A_i {B_i}^2\ \exp(B_i t)}{\left[\sum_{i=1}^{4} A_i B_i\ \exp(B_i t)\right]^2} - \frac{1}{\sum_{i=1}^{4} A_i\ \exp(B_i t)} \right\} \tag{7}$$

In all equations above A_i and B_i are the pre-exponential factors and the exponential coefficients of Eq. (1). The relations for calculating the adsorption energy ε (kJ mol^{-1}) and the modified probability density function $\varphi(\varepsilon)$ from experimental data are given by Eqs. (8) and (9):

$$\varepsilon = RT[\ln(KRT) - \ln(RT) - \ln K^\circ] \tag{8}$$

$$\varphi(\varepsilon,\ t) = \frac{\theta f(\varepsilon)}{c_{\max}^*} \tag{9}$$

where

$$f(\varepsilon) = \frac{\partial c_{\max}^*}{\partial \varepsilon} = \frac{\partial c_{\max}^* / \partial t}{\partial \varepsilon / \partial t} \tag{10}$$

The energy from lateral interactions is given by

$$\beta\theta = \frac{\theta z \omega}{RT} \tag{11}$$

The procedure of the calculation is indicated in the following diagram.

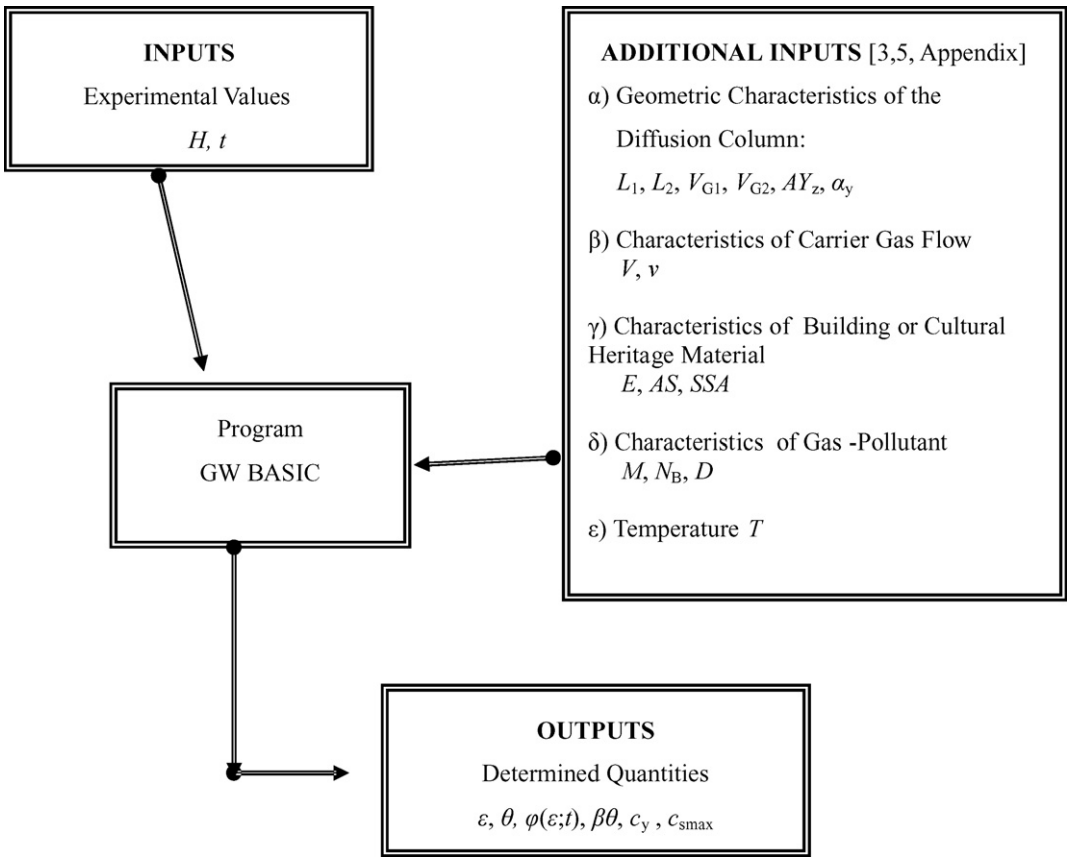

4. Results and discussion

Symmetrical and narrow extra chromatographic peaks are observed on an asymmetric continuous signal, considered as baseline. The height H, as a function of time, is measured, giving the concentration of the pollutant at $x = l'$ (Fig. 1) and time t. It is observed that the height H is a function both of the system and the time.

Using a suitable PC program the determination of the following physicochemical quantities is achieved: local adsorption energy ε, local adsorption isotherm θ, distribution function of local adsorption energy $\varphi(\varepsilon;t)$, lateral interactions $\beta\theta$, local non adsorbed gaseous concentration c_y, local monolayer capacity c_{smax}.

The local adsorption energy, ε, versus t is depicted in Fig. 5, as well as the local adsorption isotherm, θ, versus t in Fig. 6. The curves of every system gas pollutant-solid have analogous shape and their maxima and minima are observed at the same time. The minimum corresponds to the time when the monolayer coverage has been completed. This depends on the number of C atoms that the adsorbed gas has in its molecule. At the time where the maximum of the curve $\varepsilon = f(t)$ appears, minimum occurs in the diagram of distribution density function $\varphi(\varepsilon, t)$ for the respective system, as is shown in Fig. 6. That happens because the probability to find active centres with the maximum energy is very low.

Plots of distribution density function, $\varphi(\varepsilon, t)$, versus local adsorption energy, ε, are presented in Fig. 7, where the curves have the shape of a normal distribution function (Gauss), with the initial, in time, region (A) and the last (C) to be very close to the central one (B).

On the contrary, the regions A, B, C, are totally different in Fig. 8a, where the density probability function is plotted versus t, which can be explained with the mechanism of Bakaev and Steele [25], attributed to three different kinds of active centers of adsorption. Moreover, the shape of the curves remains almost stable, except for those of the marbles (Fig. 8b), where two maxima exist and the

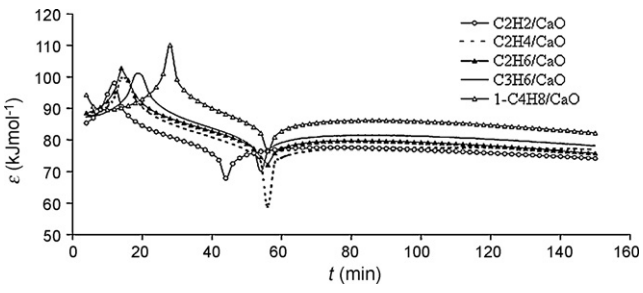

Fig. 5. Plots of local adsorption energy, ε, versus t for the systems C_2H_2/CaO, C_2H_4/CaO, C_2H_6/CaO, C_3H_6/CaO, 1-C_4H_8/CaO at 50 °C.

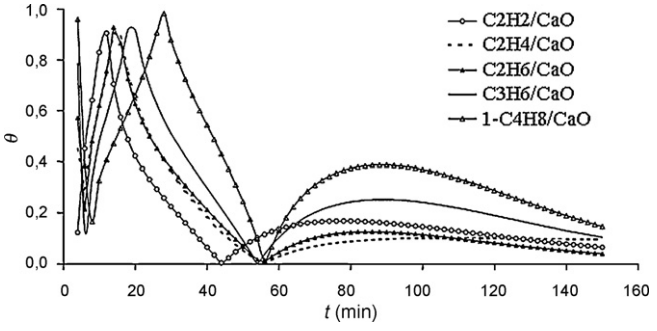

Fig. 6. Plots of local adsorption isotherm, θ, versus t for the systems C_2H_2/CaO, C_2H_4/CaO, C_2H_6/CaO, C_3H_6/CaO, 1-C_4H_8/CaO at 50 °C.

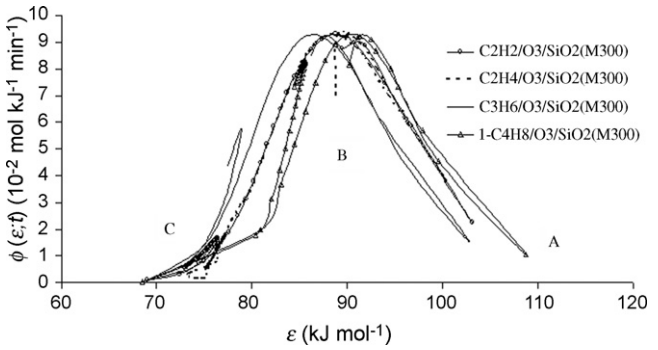

Fig. 7. Plots of distribution density function $\varphi(\varepsilon; t)$ versus local adsorption energy, ε, for the systems $C_2H_2/SiO_2/O_3/SiO_2$ (M300), $C_2H_4/O_3/SiO_2$ (M300), $C_2H_6/O_3/SiO_2$ (M300), $C_3H_6/O_3/SiO_2$ (M300), 1-$C_4H_8/O_3/SiO_2$ (M300) at 50 °C.

percentage of the active centers is much lower. The magnification indeed reveals a third region which is much lower than the first two. The value of the maximum of the third region is now relevant with the one of Fig. 8a but the area under the curve is smaller, something that means less percentage of active centers. In addition, the first two peaks in the case of marble are narrower and higher.

The results do not change significantly with the presence of O_3, but change with the presence of SO_2 (Fig. 8c). The times of maxima and minima increase from the lower molecular weight of the adsorbed gas to the higher one, under the same experimental conditions. The greater time intervals are attributed to 1-butene and the lower to acetylene. This fact is justified by the respective diffusion coefficients, since lower the diffusion coefficient, higher the respective time. A change in percentage of the region under the third maximum is presented. Furthermore, a different behavior of the solid adsorbents occurs.

The three maxima and the two minima in Fig. 8 occur in the same time with the three maxima and the two minima in the plot of the energy from lateral interactions, $\beta\theta_i$, versus t (Fig. 9).

For the plots of local adsorption equilibrium concentration, c_y, versus t (Fig. 10) it is observed for all the systems studied that the shape of the curve does not change, the slopes and the maximum values change. This curve ensues from the mathematical model, but is also the same as the so called diffusion band, which emerges directly from the experiment; a fact which shows that the results from the experiment and the mathematical model are in total agreement.

The influence of the type of the bond of the adsorbate molecules on the same adsorbent (statue) is evident. There is also a relationship between the adsorbate and the non adsorbate gas pollutant in equilibrium.

Regarding the plot of local monolayer capacity, c^*_{max}, versus t, a different behavior is observed in the presence of SO_2 (Fig. 11). In analogous experiments, in the presence of O_3, lower values for c^*_{max} are determined. This is attributed to the oxidation in homogeneous phase of hydrocarbon by O_3 before the adsorption, so lower quantities of gas are detected. Alternatively, O_3 acts competitively towards organic pollutant, as it covers active sites on the surface, which leads to lower adsorption of the organic gas.

The classification of the mineral was done according to XRD, SEM-EDAX analysis and Raman spectra.

XRD analysis was performed in the samples of marble and the statues from the Greek Archaeological Museums of Kavala and Philippi before and after the injection of the pollutants. It was found that no qualitative change occurred. As it can be seen from the XRD diagram (Fig. 12) the L351 Kavala's statue sample is a marble with major component dolomite and quite less calcite. As it can also be revealed from the XRD analysis some gypsum

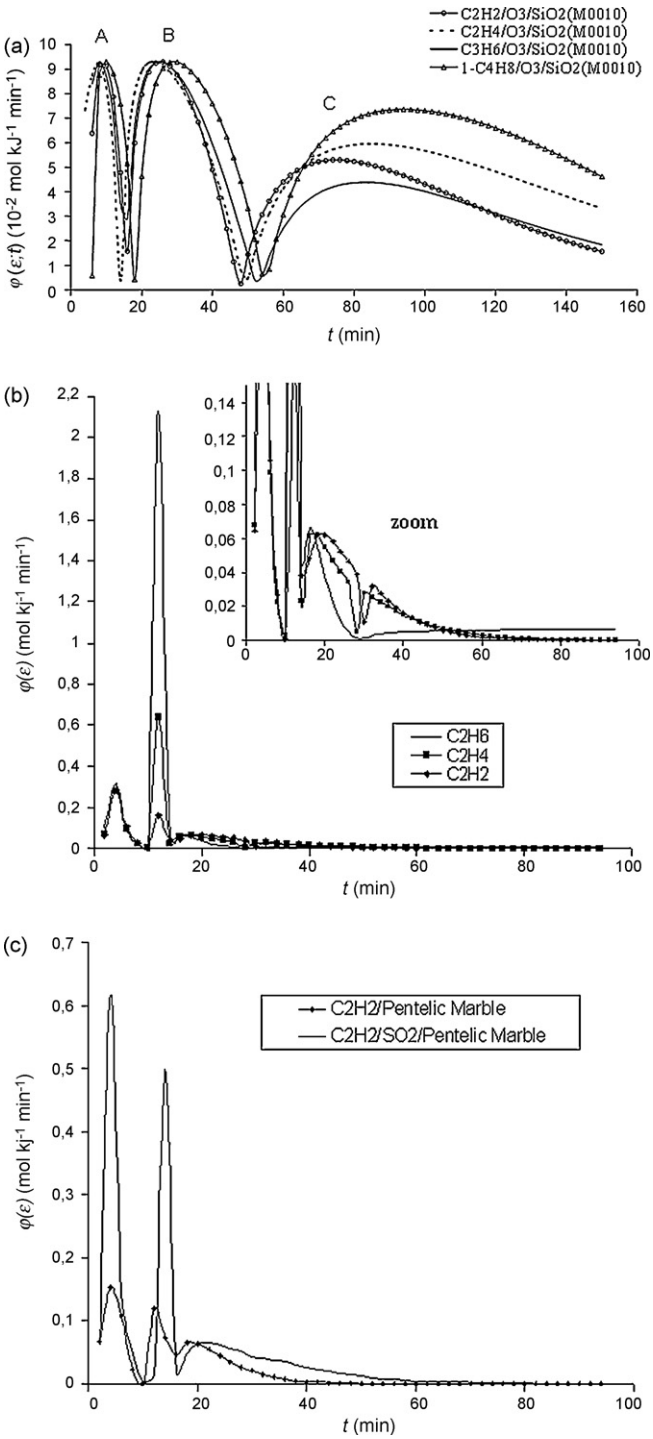

Fig. 8. Plots of distribution density function, $\varphi(\varepsilon, t)$ versus t for the systems: (a) $C_2H_2/O_3/SiO_2$ (M0010), $C_2H_4/O_3/SiO_2$ (M0010), $C_2H_6/O_3/SiO_2$ (M0010), $C_3H_6/O_3/SiO_2$ (M0010), 1-$C_4H_8/O_3/SiO_2$ (M0010), (b) C_2H_6/Statue L1991 Museum Philippi, C_2H_4/Statue L1991 Museum Philippi, C_2H_2/Statue L1991 Museum Philippi, (c) C_2H_2/Pentelic marble, C_2H_2/SO_2/Pentelic marble, at 50 °C.

was present before the exposure to the pollutants, so either the gypsum was a minor component of the marble or it was formed during previous exposure of the statue to an atmosphere that permitted this formation. After the exposure to the pollutants no gypsum was detected by any method used. This is rather expected because there was no humidity during the SO_2 contact with the marble.

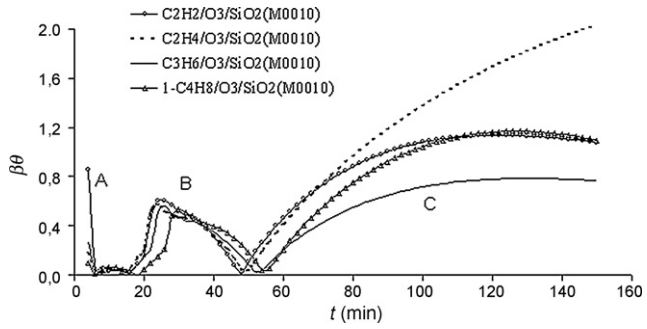

Fig. 9. Plot of energy from lateral interactions, $\beta\theta_i$, versus t for the systems $C_2H_2/O_3/SiO_2$ (M0010), $C_2H_4/O_3/SiO_2$ (M0010), $C_2H_6/O_3/SiO_2$ (M0010), $C_3H_6/O_3/SiO_2$ (M0010), 1-$C_4H_8/O_3/SiO_2$ (M0010) at 50 °C.

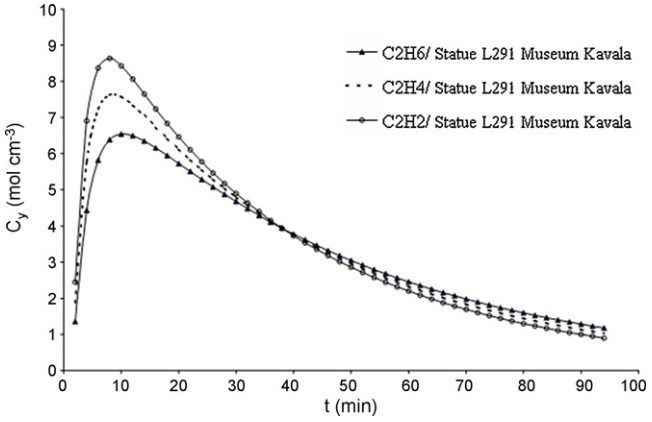

Fig. 10. Local adsorption equilibrium concentration, c_y, versus t for the systems C_2H_6/Statue L291 Museum Kavala, C_2H_4/Statue L291 Museum Kavala, C_2H_2/Statue L291 Museum Kavala.

Raman analysis was performed in the sample of statue of the Greek Archaeological Museum of Kavala before and after the influence of the hydrocarbons. Bonds of C–C και C≡C were detected, which is attributed to ethane and acetylene adsorption. More precisely, in the spectra of L351 Kavala's statue (Fig. 13) before the sample be exposed to the pollutants, it is clear that the main peak, corresponding to ν_1 symmetric stretch (A_1') of the carbonate ion, at about 1095 cm^{-1} is absent. Instead, a weak peak at approximately 998 cm^{-1} is observed, attributed to the SO_4^{-2} of the gypsum, as it was also detected by XRD. Another rather weak band at 720 cm^{-1} is due to the ν_4 vibrational mode of CO_3^{-2}. To the rotational oscillation of CO_3^{-2} about the symmetry axis is expressed by the quite strong

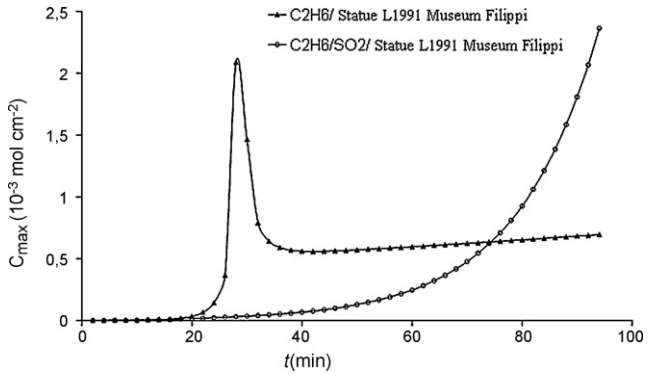

Fig. 11. Time resolved analysis of local monolayer capacity, c^*_{max}, for the systems C_2H_6/Statue L1991 Museum Philippi, C_2H_6/SO_2/Statue L1991 Museum Philippi.

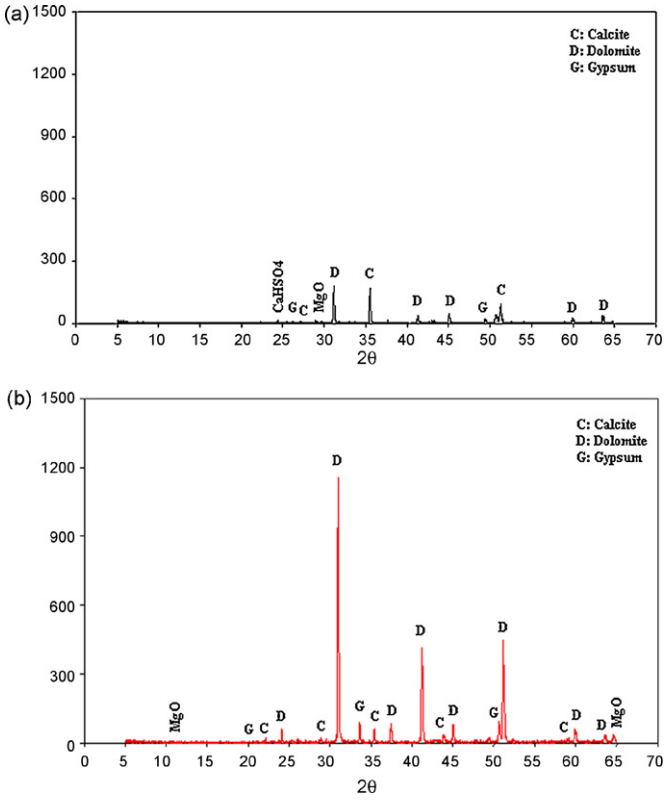

Fig. 12. XRD diagram for the Statue L351 Museum Kavala (a) before and (b) after the influence of air pollutants.

band at 90–125 cm^{-1}. The very weak peaks at 1640–1660 cm^{-1} and 1745–1750 cm^{-1} are attributed to a stretching vibration of C=C and C=O respectively. Other two very weak peaks are observed at the end of the right side spectra at 2884 cm^{-1} and at 3103 cm^{-1}. The former is due to the presence of n-alkanes and the later is attributed to the anti-symmetric vibration of $=CH_2$, present in C_2H_4. After the exposure, at the left end of spectra the two medium bands present at 150–190 cm^{-1} and 280–300 cm^{-1} are attributed to the interactions between cation and anion. The main peak of CO_3^{-2} at 1095 cm^{-1} is present. All the other weak peaks have been smoothed and a band at 1970–2200 cm^{-1} is distinguished. This

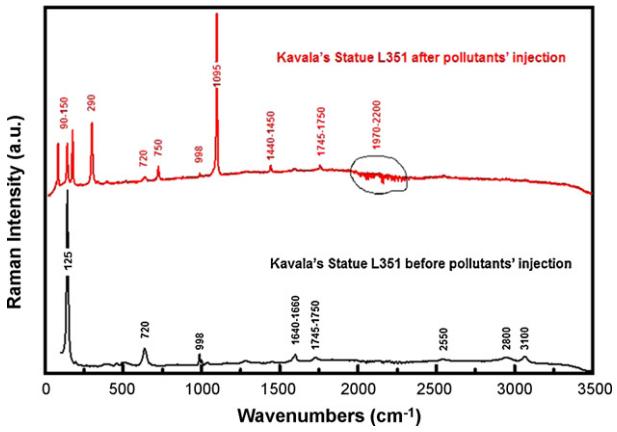

Fig. 13. Raman spectra from a sample of statue from Museum of Kavala, before (black line) and after (red line) the influence of air pollutants. (For interpretation of the references to color in this figure legend, the reader is referred to the web version of the article.)

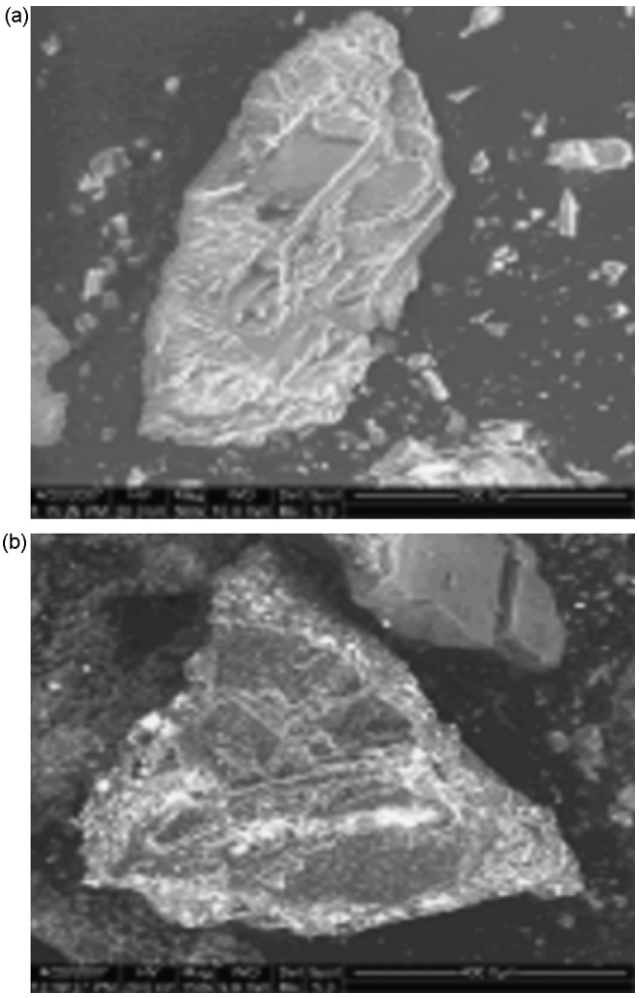

Fig. 14. SEM images showing the shapes of (a) calcite and (b) dolomite.

band is not signed by the intensity of the peaks, but as a number of them. This band is due to the C_2H_2. From the combination of Raman and SEM-EDAX analysis, SO_2 was found, showing that it was adsorbed.

Last but not least Fig. 14a and b shows the difference between a grain of calcite and dolomite. The dolomite sample seems to be better adsorbent than the calcite ones. This property of dolomite is attributed to its more coarse crystallites, as it can be seen in SEM micrographs. Calcite's aspect is more tight and compact while the one of dolomite seems to be more porous.

It is evident that RF-IGC method combined with a suitable mathematical model, provides a valuable tool, in a modern laboratory, in order to investigate the impact of atmospheric pollution on solids. A significant finding is that, in this case, all local physicochemical quantities are obtained experimentally.

The methods used at the second part of this study, have been selected in order to reveal the components' nature of marbles and statues before exposure and to detect any differentiation after that. It was also an attempt to cross over the results of RF-IGC with these of the used classical methods.

From this part it is also confirmed that the gas pollutants are adsorbed from the marbles and statues with different rates and especially C_2H_2 is the most retained on them. This is a fact that explains the synergy between SO_2 and C_2H_2 and shows that C_2H_2 collaborates better with SO_2, which it seems to be the "bridge" between marble and C_2H_2.

5. Conclusions

In order to investigate the impact of air pollution on building materials as well as on authentic samples of Greek statues, providing at the same time a scientific platform to conservation procedures, the method of RF-IGC has been used. It is the adsorption phenomenon that has been studied both experimentally and through suitable mathematical models. The all phenomenon has been investigated qualitatively and quantitatively with different pollutants. The synergistic effect of a second pollutant has also been examined. Thus, the SO_2 favors the adsorption of all hydrocarbons studied, but especially this of acetylene. On the contrary, O_3 acts competitively towards organic pollutant, as it covers active sites on the surface, which leads to lower adsorption of the organic gas. The time-resolved chromatographic analysis focuses on expressing the pollutant impact, in physicochemical terms, in order to study the deterioration mechanism, in detail. When the deterioration mechanism is well known, then the effective conservation of monuments of cultural heritage can be approached. The XRD, SEM-EDAX and Raman analysis revealed the components' nature of marbles before and after the exposure to the pollutants. It was also confirmed that dolomite adsorbs more than the other and the more retained gas was the acetylene. The dolomite sample seems to be better adsorbent than the calcite ones. This property of dolomite is attributed to its more coarse crystallites.

Acknowledgments

The authors acknowledge the financial support under the research program PYTHAGORAS II 2005–2006. The project is co-funded by the European Social Fund (75%) and National Resources (25%).

Special thanks to the Archeological Museums of Kavala and Philippi for the kindly supply of statue samples, after permission from the Greek Ministry of Culture.

Appendix A

L_1	length of the empty section z of diffusion column (cm)
L_2	length of the filled section y of diffusion column (cm)
V_{G1}	gaseous volume of the empty column L_1 (cm^3)
V_{G2}	gaseous volume of the filled column L_2 (cm^3)
AY_z	cross sectional area of section L_1 (cm^2)
α_y	cross sectional area of the void space in region y (cm^2)
V	volumetric flow-rate of carrier gas ($cm^3\ min^{-1}$)
v	linear flow velocity of carrier gas ($cm\ s^{-1}$)
E	external porosity (dimensionless)
AS	mass of adsorbate per height ($g\ cm^{-1}$)
SSA	specific surface area ($cm^2\ g^{-1}$)
M	molar mass of the adsorbate ($kg\ mol^{-1}$)
N_B	amount of adsorbate injected (mol)
D	diffusion coefficient of gas adsorbate into the nitrogen carrier gas ($cm^2\ s^{-1}$)
T	temperature (K)

References

[1] N.S. Baer, F.N. Banks, Indoor air pollution: effects on cultural and historic materials, Int. J. Museum Manage. Curatorship 4 (1985) 9–20.
[2] P. Bimblecombe, The composition of museum atmospheres, Atmos. Environ. 24B (1990) 1–8.
[3] N.A. Katsanos, F. De Santis, A. Cordoba, F. Roubani-Kalantzopoulou, D. Pasella, Corrosive effects from the deposition of gaseous pollutants on surfaces of cultural and artistic value inside museums, J. Hazard. Mater. A 64 (1999) 21–36.

[4] A.V. Dremetsika, P.A. Siskos, N.A. Katsanos, Determination of adsorption entropies on solid surfaces by reversed-flow gas chromatography, J. Hazard. Mater. 149 (2007) 603–608.
[5] D. Dragovich, Marble weathering in an industrial environment, Eastern Australia, Environ. Geol. Water Sci. 17 (1991) 127–132.
[6] P. Kirkitsos, D. Sikiotis, Deterioration of Pentelic marble, Portland limestone and Baumberger sandstone in laboratory exposures to NO_2: a comparison with exposures to gaseous HNO_3, Atmos. Environ. 30 (1996) 941–950.
[7] F. De Santis, V. Di Palo, I. Allegrini, Determination of some atmospheric pollutants inside a museum: relationship with the concentration outside, Sci. Total Environ. 127 (1992) 211–223.
[8] R. Van Grieken, F. Delalieux, K. Gysels, Cultural heritage and the environment, Pure Appl. Chem. 70 (1998) 2327–2331.
[9] D. Brocco, A. Giovagnoli, M. Tabasso, Laurenzi, M. Marabelli, R. Tappa, R. Polesi, Air pollution in Rome and its role in the deterioration of porous building materials, Durability Building Mater. 5 (1988) 393–403.
[10] S. Lorusso, C. Fiori, A. Tucci, E. Rastelli, D. Pinna, Study on the conservation of the medicean walls of terra del sole (Forlì Italy), C e Ca 34 (2004) 207.
[11] P. Elfving, I. Panas, O. Lindqvist, In situ IR study on the initial sulphition and carbonation of $Ca(OH)_2$ and CaO by SO_2 polluted air, Atmos. Environ. 30 (1996) 4085–4089.
[12] F. Roubani-Kalantzopoulou, T. Agelakopoulou, I. Bassiotis, S. Margariti, V. Siokos, E. Metaxa, Influence of nitrogen dioxide and acetylene on marbles, ceramics and pigments, Global. NEST. J. 10 (2008) 183–191.
[13] E. Metaxa, T. Agelakopoulou, I. Bassiotis, S. Margariti, V. Siokos, F. Roubani-Kalantzopoulou, Time-resolved gas chromatography applied to submonolayer adsorption. Modeling and experimental approach, Appl. Surf. Sci. 253 (2007) 5841–5845.
[14] T. Agelakopoulou, I. Bassiotis, E. Metaxa, F. Roubani-Kalantzopoulou, Benzene and toluene influence with or without nitrogen dioxide, Atmos. Environ. 41 (2007) 2009–2018.
[15] N.A. Katsanos, G. Karaiskakis, Time-Resolved Inverse Gas Chromatography and Its Applications, HNB Publishing, 2004.
[16] N.A. Katsanos, F. Roubani-Kalantzopoulou, Advances in physico-chemical measurements using inverse gas chromatography, Adv. Chromatogr. 40 (2000) 231–273.
[17] F. Roubani-Kalantzopoulou, Determination of isotherms by gas–solid chromatography applications, J. Chromatogr. A 1037 (2004) 191–221.
[18] N.A. Katsanos, E. Arvanitopoulou, F. Roubani-Kalantzopoulou, A. Kalantzopoulos, Time distribution of adsorption energies, local monolayer capacities and local isotherms on heterogeneous surfaces by inverse gas chromatography, J. Phys. Chem. B 103 (1999) 1152–1157.
[19] N.A. Katsanos, E. Iliopoulou, F. Roubani-Kalantzopoulou, E. Kalogirou, Probability density function for adsorption energies over time on heterogeneous surfaces by inverse gas chromatography, J. Phys. Chem. B 103 (1999) 10228–10233.
[20] D. Gavril, An inverse gas chromatographic tool for the measurement of local isotherms on heterogeneous surfaces, Instrum. Sci. Technol. 30 (2002) 409–425.
[21] N.A. Katsanos, F. Roubani-Kalantzopoulou, E. Iliopoulou, I. Bassiotis, V. Siokos, M.N. Vrahatis, V.P. Plagianakos, Lateral molecular interaction on heterogeneous surfaces experimentally measured, Colloids Surf. A 201 (2002) 173–180.
[22] D. Gavril, A. Koliadima, G. Karaiskakis, Adsorption studies of gases on Pt–Rh bimetallic catalysts by reversed flow gas chromatography, Langmuir 15 (1999) 3798–3806.
[23] F. Roubani-Kalantzopoulou, I. Bassiotis, Th. Artemiadi, S. Margariti, E. Arvanitopoulou, N.A. Katsanos, Simulation of the physicochemical processes in the atmosphere, Fresenius Environ. Bull. 10 (2001) 98–102.
[24] F. Roubani-Kalantzopoulou, Th. Artemiadi, I. Bassiotis, N.A. Katsanos, V.P. Plagianakos, Time separation of adsorption sites on heterogeneous surfaces by inverse gas chromatography, Chromatographia 53 (2001) 315–320.
[25] V.A. Bakaev, W.A. Steele, Computer simulation of the adsorption of argon on the surface of titanium oxide. 1. Crystalline rutile, Langmuir 8 (1992) 1372–1378.